Influence of dielectric thickness and electrode structure on the ion wind generation by micro fabricated plasma actuators

To cite this article: R Hink *et al* 2020 *J. Phys. D: Appl. Phys.* **53** 405201

OPEN ACCESS
IOP Publishing
Journal of Physics D: Applied Physics
J. Phys. D: Appl. Phys. **53** (2020) 405201 (10pp)
https://doi.org/10.1088/1361-6463/ab96ea

Influence of dielectric thickness and electrode structure on the ion wind generation by micro fabricated plasma actuators

R Hink[1], A V Pipa[1], J Schäfer[1], R Caspari[2], R Weichwald[2], R Foest[1] and R Brandenburg[1]

[1] Leibniz Institute for Plasma Science and Technology, Greifswald, 17489, Germany
[2] Airbus Defence and Space, Manching, 85077, Germany

E-mail: pipa@inp-greifswald.de

Received 6 February 2020, revised 7 May 2020
Accepted for publication 27 May 2020
Published 17 July 2020

Abstract

Surface dielectric barrier discharges are investigated in order to explore the combined effects of barrier thickness and microstructure of the exposed electrode on the ion wind generation. Actuators with straight and structured high voltage electrodes with characteristic sizes of 200 and 250 μm and dielectric thicknesses of 0.5, 1 and 2 mm are compared. It is observed that: i) actuator efficiency of ion wind generation strongly depends on the applied voltage amplitude; ii) operation voltage depends on the dielectric thickness logarithmically; iii) electrode microstructure slightly increases the dynamic pressure (few percent in maximum), however the effect decreases with thicker dielectrics and smaller electrode structures; iv) the pattern of the most intensive discharge parts as well as the dielectric erosion repeats the regular structure of the electrodes down to 200 μm. Several identical samples are tested during different days to estimate the impact of the air humidity and the degradation of the dielectric. The microscale precision of the sample manufacture was accomplished by a commercial facility for printed circuit boards.

Keywords: surface dielectric barrier discharge, plasma actuators, microstructure, dielectric thickness, ion wind, pitot tube, active flow control

(Some figures may appear in colour only in the online journal)

1. Introduction

The growing demand on passenger aircraft and the limitation of air transportation and finite fossil fuels require fuel-saving technologies. During the last decade, the flow control by non-thermal plasma with asymmetric surface dielectric barrier discharges (SDBDs) was extensively investigated as drag reduction technology for aerospace applications [1–7]. These devices are also called plasma actuators. SDBDs have typically two electrodes fixed on the opposite sites of a dielectric barrier, the so-called top or exposed electrode and the lower or embedded electrode. A discharge initiates at the edge of the exposed electrode and expands over the dielectric surface in the area above the embedded electrode. The SDBD induces an airflow above the surface named as electric or ion wind. Typical applied voltage amplitudes are between 5 and 35 kV and frequencies in the kHz range [1]. The induced flow can prevent a boundary layer separation at aircraft wings and enable higher angles of attack [8]. The use of SDBDs can also damp Tollmien-Schlichting waves [9] and thus, delay the boundary layer transition from laminar to turbulent, which leads to a

local reduction of the drag by up to 50% [10]. The discharge operates successfully at reduced pressure [11], e.g. at flight altitude of commercial passenger aircrafts. The boundary layer transition delay was also tested successfully under flight conditions [12]. In addition, SDBDs looks promising for the deicing of aircraft surfaces [13].

The ion wind velocity increases with the amplitude of applied voltage up to a certain voltage threshold at which the velocity grows less significantly [14]. This saturation voltage depends on the voltage waveform, the frequency as well as on geometry of the discharge. The highest measured ion wind velocity for a single SDBD was reported by Benard *et al* [1] with a value of 7 m s^{-1} by using a 4 mm thick dielectric and 1 kHz frequency of the applied voltage amplitude of 30 kV. The same authors also reported a maximum ion wind velocity for a multi SDBD arrangement with four SDBDs in a row of 10.5 m s^{-1} by using a 3 mm thick dielectric and 1 kHz frequency of the applied voltage amplitude of 24 kV. A thick dielectric and a low frequency lead to higher saturation voltages and were recommended in order to reach the maximum thrust by the ion wind [1, 14, 15]. High voltage amplitudes and large dielectric thicknesses complicate the implementation of the actuators to flow control applications. Therefore, effective generation of significant ion wind at low voltages using thin and thus, flexible dielectric surfaces is a current demand. The optimization of the discharge geometry still provides wide opportunities for further improvements of SDBD actuators [14, 16]. Two linear actuators working in opposite direction provide ion wind in the direction perpendicular to the dielectric, which can be enhanced in annular geometry [16]. Stair-wise shaped dielectric [5] and paired electrode design [5, 17] can improve actuator efficiency. In the present work we focus on the shape of the high voltage electrode in combination with the dielectric thickness.

Thomas *et al* [14] showed that the thrust increases for structured electrodes in comparison to straight electrodes. The effect is decreasing with the voltage amplitude, but more than 30% gain of thrust was measured at a voltage amplitude of about 20 kV (40 kV_{PP}). In the study of Thomas *et al* an isosceles triangle electrode structure was investigated with a base length of 3.2 mm and a height of 12.7 mm. Debien *et al* [18] pointed out that the use of a 13 μm wire as exposed electrode increases the thrust by more than 25% in comparison to a 300 μm wire. Abe *et al* [19] also demonstrated that smaller electrode thickness and a fine structured electrode enhance ion wind generation. Also it was concluded that a microstructured electrode edge, fabricated from thin wire mesh, can increase ion wind thrust in 50% at atmospheric pressure in comparison to a straight tape electrode of the same thickness.

The decrease of the dielectric thickness leads to an increase of the electric field and consequently results in discharge ignition at lower voltage amplitudes. Forte *et al* showed [15] that at low voltage amplitudes thinner dielectrics result in higher maximum velocities of the ion wind. However, for a significant flow control effect a sufficiently high voltage amplitude is required. This restricts the minimum thickness because the dielectric has to resist against the electrical breakdown.

The role of both parameters—the size of the microstructured electrode and the dielectric thickness—on the ion wind generation as well as their combination are investigated in this study. Actuators with straight and structured (right-angled triangles with base lengths of 200 and 250 μm) electrodes with dielectric thicknesses of 0.2, 0.5, 1 and 2 mm are studied. Attention is given to the reproducibility of the measured effects by the examination of several microfabricated samples of the same design produced by a commercial printed circuit board manufacturer. The size of the investigated structures is significantly smaller than the one of Thomas *et al* [14]. The structure of rectangular isosceles triangles is characterized by a single parameter, namely, the distance between them. In addition, the manufacturing process for the structured and straight electrodes allows a gradual transition between them in contrast to Abe *et al* [19]. Indeed, the fabrication of the electrode microstructures by semiconductor fabrication techniques, e.g. for micro-electro-mechanical systems (MEMS) [20, 21] would be feasible and would enhance the precision. However, the enhanced effort (e.g. cleanroom facilities, processing time, advanced etching techniques) is not justified and economically unreasonable for the small number of specimen.

The ion wind is characterized by means of measured dynamic pressures. The flow velocity is not used for characterization. It has a square root dependence on the dynamic pressure and therefore, it is less sensitive to the observed effects. In addition, the dynamic pressure behaves proportional to the actuator thrust. Latest studies show a strong degradation of organic materials like the often used polyimides (e.g. Kapton®) [22]. Therefore, and considering our own observations, the surface and electrode degradation by the plasma operation was investigated using a scanning electron microscope (SEM).

2. Experimental setup

Printed circuit boards (PCB) with an area of 80 x 80 mm from IBR Leiterplatten GmbH & Co. KG were used as a base for the SDBDs. The dielectric material is woven fiberglass embedded in resin (FR-4 TG135) with thicknesses of 0.2, 0.5, 1.0 and 2.0 mm. However, the samples with a thickness of 0.2 mm were not sufficiently robust for systematic measurements due to the fast degradation of the dielectric in contact with the plasma. The design of the top (brown) and bottom (blue) electrode of the PCBs are shown in figure 1. The high voltage electrodes (brown) have three different shapes at the connection line to the ground electrode (blue). One shape of the electrode is straight. The others have right-angled triangles with base lengths of 200 and 250 μm as shown in figure 1(b). All electrodes consist of a 35 μm thick copper layer with a chemical gold coating for passivation.

The power supply was a AC source (Chroma, model 61 604) providing a 1 kHz sinus shaped waveform to a custom-built transformer (Bremer Transformatoren GmbH) supplying a maximum amplitude of up to 10 kV. The discharge was operated in ambient air at atmospheric pressure.

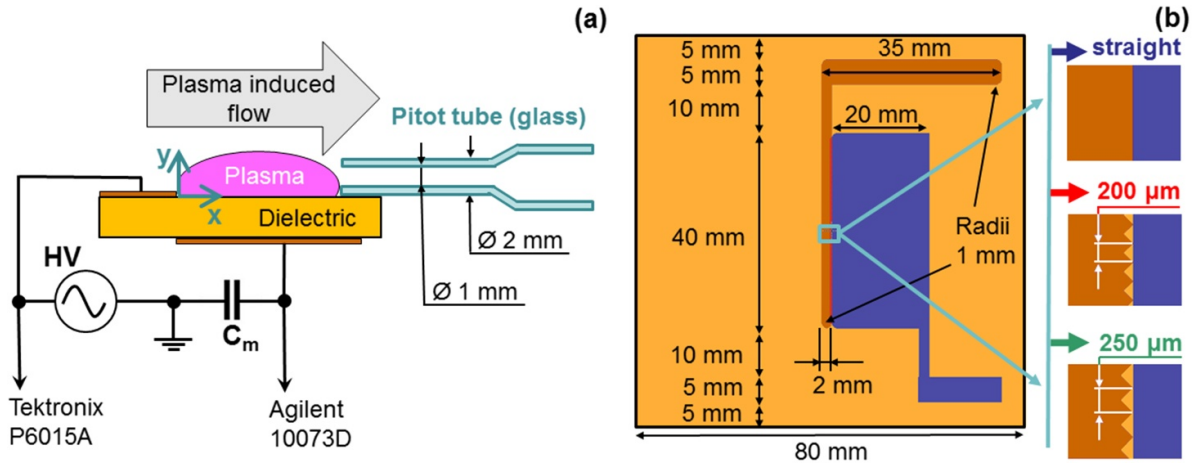

Figure 1. Experimental setup (a) and printed circuit boards design (b).

The high voltage was measured using a Tektronix P6015A 1:1000 high voltage probe. The charge transferred in the gas gap of the SDBDs was determined by use of a Mica CD19 capacitor (Cornell-Dubilier, $C_m = 1$ nF $\pm$ 1% tolerance with), see figure 1(a), connected to an Agilent 10 073D 1:10 probe. The voltage probes were coupled to an oscilloscope (Agilent DSO 7032B), which also averaged the charge-voltage plot of the samples over 100 high voltage cycles. The charge-voltage characteristics were integrated to obtain the dissipated power of the SDBDs. For further details on the technique of power measurements see [23] and references therein.

The ion wind was quantified by measurements of the dynamic pressure by a Pitot tube connected to a MKS Instruments 120AD Baratron, which is a high-accuracy capacitance differential manometer, and a MKS Instruments 651 C control unit. The quartz Pitot tube had an inner diameter of 1 mm and an outer diameter of 2 mm. The inner tube diameter of 1 mm covered at least four triangles of the microstructured electrodes, so that no influence by the structure in the Pitot pressure could be measured along the electrode. The Pitot tube was aligned on the dielectric surface ($y = 0$ mm). The ion wind above the surface is always influenced by boundary layer effects, e.g. friction. For typically investigated SDBDs friction effects are mainly obtained at wall distances below $y = 0.5$ mm, e.g. Jolibois and Moreau [24] or Kriegseis *et al* [25]. The Pitot tube in the present work integrated the ion wind within distance y of 0.5 and 1.5 mm from the dielectric surface and, therefore, should capture its maximum, except in the region at close vicinity to the electrodes.

A micrometer-screw translation stage (OWIS) was used to move the Pitot tube along dielectric surface. The dynamic pressure quickly grows with the distance from the high voltage electrode until a maximum is reached and then gradually decreases. Thus, the measurements of the dynamic pressure behind the maximum are much less sensitive to the positioning of the Pitot tube. Most of the measurements were performed at the position $x = 7$ mm which is just behind the maximum of the dynamic pressure for all investigated conditions as shown by the coordinate system in figure 1.

The Pitot tube measurements provide the values of the dynamic pressure p_d, which is related to the ion wind velocity v by Bernoulli's equation. If the laboratory conditions are assumed as: $T = 296$ K and $p = 1013$ mbar, that leads to an ambient air density $\rho_{air} \approx 1.19$ [$kg{\cdot}m^{-3}$] and ion wind velocity can be computed as:

$$v[\mathrm{ms}^{-1}] = \sqrt{\frac{2p_d}{\rho_{air}}} \approx 1.3\sqrt{p_d[\mathrm{Pa}]}. \quad (1)$$

The upper pressure limit of the used differential manometer is about 10 Pa, which corresponds to an ion wind velocity of about 4 m s^{-1}. This was sufficient for most measurements limited by amplitude of the applied voltage of 10 kV (≈ 7.1 kV$_{RMS}$). Forte *et al* [15] reports a maximum measured velocity of 3 m s^{-1} for a similar setup with 7 kV$_{RMS}$, 1 kHz and a 1 mm thick PMMA plate as dielectric, which is inside the upper limit of the used devices and also agrees with the data of this study.

3. Experimental results

3.1. Discharge appearance

The appearance of the discharge was photographed with a Canon EOS 77D camera and a Tamron objective with 18-200 mm focal length and 10 s exposure time (vibrational compensation was turned off). Selected parts of the pictures, corresponding to 1x10 mm actuator area are presented in figure 2. At the maximum applied voltage, see figure 2(b), the discharge expands almost 7 mm outwards of the high voltage electrode edge. The most intense parts of the discharge are located in the vicinity of the electrode edge and their shape depends on the electrode structure. The edge of the straight electrode is illuminated homogeneously and it is seen as a bright straight line. The edge of the 200 μm structured electrode contains five bright spots situated along 1 mm electrode

Figure 2. Top view of electrode structure photographed by Canon EOS 77D under 1.8 kV$_{RMS}$ (a) and 7.0 kV$_{RMS}$ (b) operation voltage, 0.5 mm samples.

length equidistantly. The edge of the 250 μm structured electrode contains four spots with similar brightness. The positions of these spots represent the protruding tips of the triangles of the electrode structure, which have the smallest distance to the ground electrode. The discharge develops towards the electrode. Furthermore, a weak emission is also present above the electrode. In the case of the 250 μm structure the discharge in the opposite direction of the main discharge above the upper electrode is less pronounced.

In figure 2(a) discharge photographs are presented at an applied voltage of 1.8 kV$_{RMS}$ which is slightly above the ignition voltage of about 1.5 kV$_{RMS}$. Irregular bright spots are present on the edge of the straight electrode indicative of the filamentary nature of the surface discharge. At low voltages, preferred locations of the filaments can be detected with the 10 s exposure time, whereas at high voltage the large amount of erratically distributed filaments leads to the impression of a uniform plasma. The structured electrodes have bright spots at the same positions, but, at low voltages the brightness varies from spot to spot. Probably, the electrode defects have a smaller influence at higher voltages and the discharge spreads more regular.

The SDBD has a filamentary behaviour (streamer mechanism) in general as recognized by short pulses on the current waveforms and by high-speed camera photos, see for example [2, 16]. The random appearance distribution of the filaments results in an uniform appearance if the photo exposure time covers about 10^4 high voltage cycles as in figure 2. However, if the applied voltage is too high, the SDBD can turn to the saturation regime, when a further increase of the power does not enhance the ion wind and the discharge will not appear uniform anymore [14]. This saturation regime was never reached in present work since the maximum high voltage was limited to 10 kV (7.1 kV$_{RMS}$). This value is below the saturation threshold.

3.2. Electrode structure effect for 0.5 mm dielectric

In figure 3 the results of four sets of measured plasma power and dynamic pressure data are shown. Every set contains the data of three individual SDBD samples with a straight, a 200 μm and a 250 μm structured high voltage electrode, respectively. The samples in one set were investigated sequentially within four hours in order to minimize effects of the changing ambient humidity. The high voltage was applied only for a short period of time that was necessary to record the measurements (about a minute for each point). Such minimization of the operation time reduces the degradation of the dielectric. The voltage was increased stepwise from 0 up to 7.2 kV$_{RMS}$ and then it was decreased with the same step size of about 0.7 kV$_{RMS}$. The voltage of 1.5 kV$_{RMS}$ is just below the discharge ignition voltage for the samples of 0.5 mm thickness.

Figure 3(a) elucidates the influence of the electrode structure for every set. In one measured set the consumed power agrees within an experimental error of about 5% for all electrode structures. The dynamic pressure shows a similar trend, but the data for the 250 μm structured electrodes exhibit systematically highest values followed by the 200 μm structured electrodes and the lowest values are found for the straight electrodes.

All measured power values are plotted together in figure 3(b) indicating the day-to-day variation, which is most likely correlated with the ambient air humidity, see inset in figure 3(b). All dynamic pressure values are shown in figure 3(c) underlining that the electrode structure has a slight effect on the ion wind generation while the influence of the humidity is less pronounced, see the inset in figure 3(c).

3.3. Dielectric thickness

The data for SDBD samples with different dielectric thicknesses are displayed in figure 4. The measured powers and ion wind induced dynamic pressures for 1 and 2 mm thick PCBs are shown in figure 4(a) as a function of the applied voltage. The structured electrodes show systematically higher values of the dynamic pressure similar to the 0.5 mm samples, but, this feature is decreasing with the thickness of the dielectric. The pressures generated by micro-structured electrodes are systematically higher by a few percent compared to the straight electrodes. However, these values are within the experimental error. To show this effect more clearly, the dynamic pressure is plotted versus the consumed power in figure 4(b). The data points for the 200 μm structured electrodes were fitted by polynomial functions for all thicknesses and only the fits are displayed for better visibility. The data points for the straight electrode are below the curve or coincide with it, whereas the data points for the 250 μm structured electrode are on the curve or above it. This difference is more pronounced for 0.5 mm thick samples in comparison to 2 mm samples. The data for samples with 1 mm thickness are not presented in the figure but also confirm this trend.

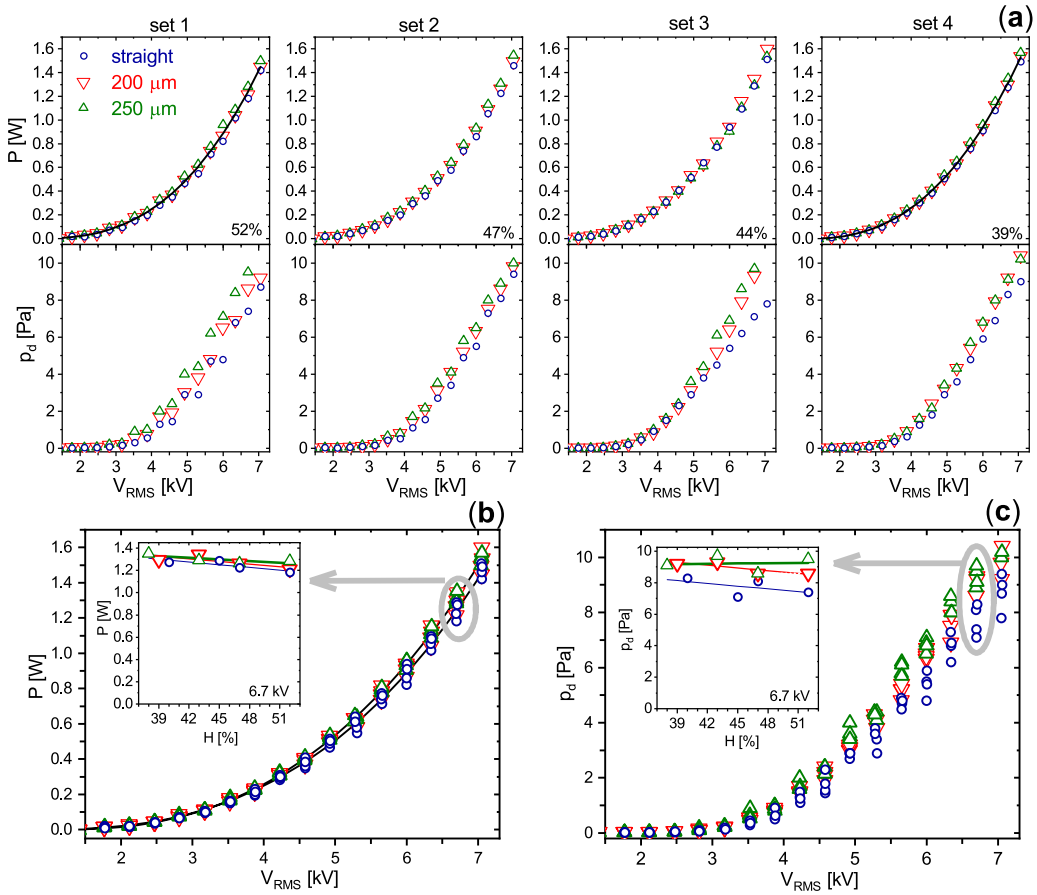

Figure 3. Measured dissipated power and dynamic pressure as a function of the applied voltage for different structures of the electrode: circles–straight, up triangles—250 μm structure and down triangles—200 μm structure. (a) Comparison of a sample set measured during one day. Four sets were measured in different days with a relative humidity of the ambient air of about 52, 47, 44, and 39%. All measured points of the set 1 and 4 were fitted by polynomial functions shown by the solid lines. All power and dynamic pressure data are displayed together in (b) and (c), respectively. Insets display the data for an applied voltage of 6.7 kV as a function of the relative humidity H. The straight lines are linear fits for each sample.

The absolute values for the power and the dynamic pressure decrease with increasing dielectric thickness for the same applied voltages, see figures 3 and 4(a). The 2 mm thick samples at the maximum applied voltage of 7 kV_{RMS} generate dynamic pressures about 3± 1 Pa, whereas for 1 and 0.5 mm thick samples it requires only 6 and 5 kV_{RMS} respectively. Thus, a thinner dielectric allows operating the SDBD at lower voltages. The direct comparison of the dynamic pressures generated by the 200 μm structured samples with different thickness is shown as a function of voltage in figure 5(c). The idea of the analysis was to compensate the effect of the different dielectric thicknesses on the ion wind generation by a re-scaling of the applied voltage value. It was found that a multiplication of the voltage with a factor of 1, 1.15 and 1.3 for 2, 1 and 0.5 mm thick samples, respectively, merges the measured data to the same function, see figure 5(d). This scaling procedure is described by the following empiric relation between the operation voltages V_0 and V_d applied for the generation of the same air flow at SDBDs with thickness d_0 and d respectively:

$$\frac{V_0}{V_d} = 1 + \frac{1}{2} log_{10}\left(\frac{d_0}{d}\right). \qquad (2)$$

The fact that doubling of the dielectric thickness requires an increase of the operation voltage amplitude of about 15% for the generation of the same dynamic pressure can be related to peculiarities of our set up, in particular the type of dielectric and the electrode design. Thus, for our case, the logarithm was multiplied on constant 1/2. We assume that the logarithmic dependence of the operation voltage on dielectric thickness similar to equation (2) can be applied for other actuators if the constant in front of logarithm will be properly adjusted.

3.4. *Efficiency of the ion wind generation*

The actuator efficiency is estimated by the ratio of the dynamic pressure to the consumed electrical power (p_d/P). Figure 5 illustrates the influence of the dielectric thickness on the ratio p_d/P for all electrode structures. Here, p_d/P is plotted as a function of power (a), voltage (b) and distance from the high voltage electrode (c). In figure 5(a), the ratio p_d/P is plotted for the straight and 250 μm structured electrodes. Samples with a thicker dielectric have the advantage of a higher efficiency at

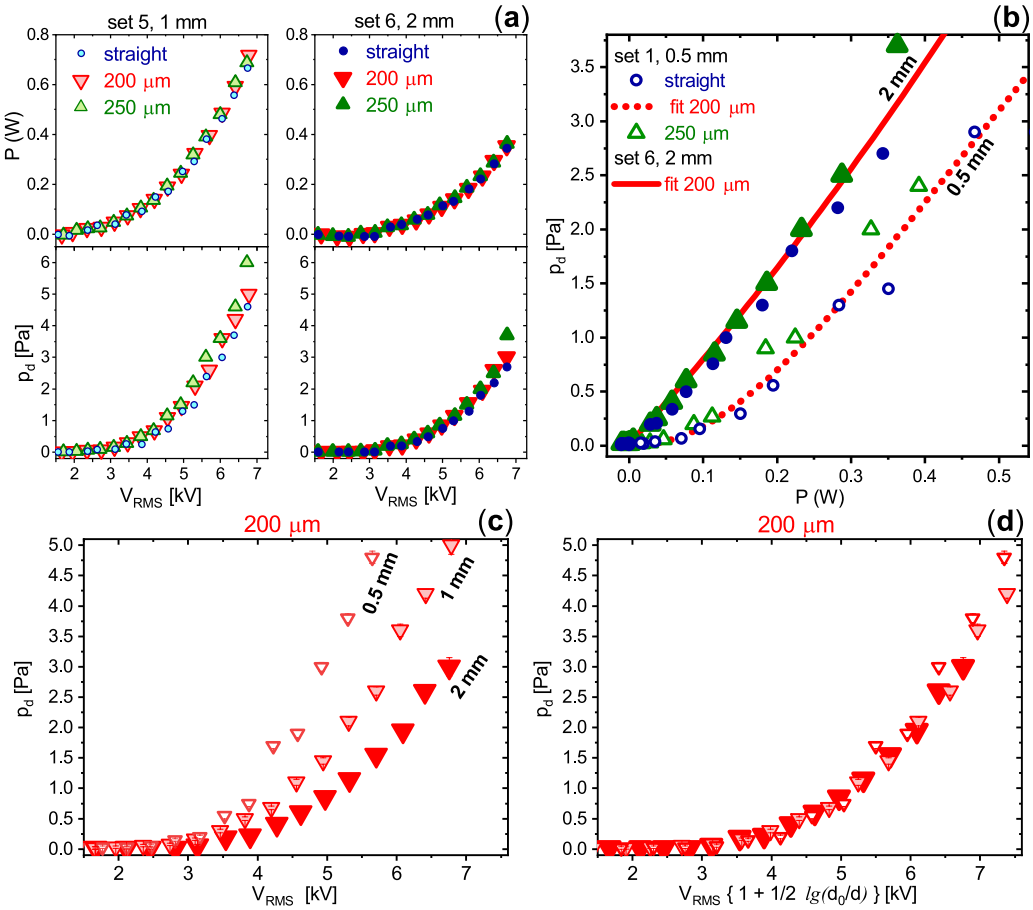

Figure 4. Dissipated power and dynamic pressure for different PCB thicknesses. (a) Direct measurements for set 5 and 6 with PCB 1 and 2 mm respectively. (b) Dynamic pressure as a function of power for set 1 (0.5 mm) and set 6, the data for 200 μm structure are presented as a polynomial fit of the measured points. (c) The direct measurements for 200 μm structure for all dielectric thicknesses. (d) The same data as in (c) with rescaled x-axis for 1 and 0.5 mm thick samples ($d_0 = 2$ mm).

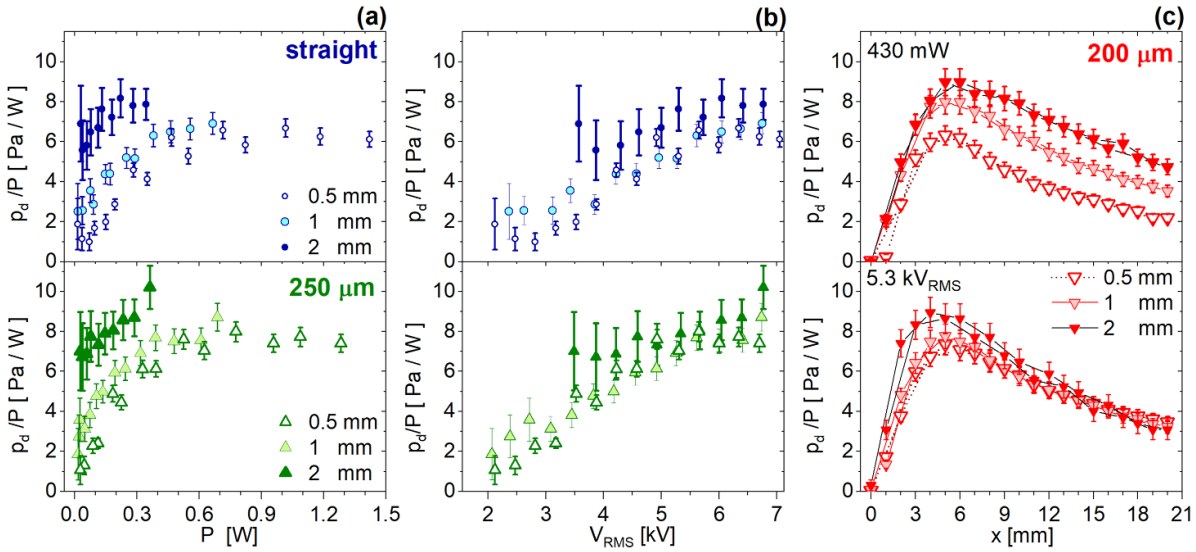

Figure 5. Dynamic pressure per dissipated electrical power as a function of (a) power, (b) applied voltage and (c) distance from high voltage electrode for thicknesses of the circuit boards of 0.5 mm (open symbols), 1 mm (shadowed symbols) and 2 mm (dark symbols). Circles represent straight electrodes, down triangles are 200 μm and up triangles are 250 μm structured electrodes.

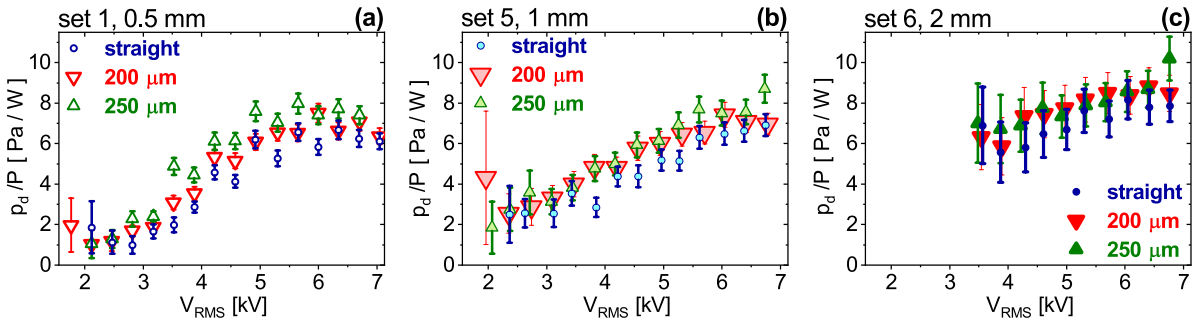

Figure 6. Dynamic pressure per dissipated electrical power as a function of applied voltage for dielectric thickness of (a) 0.5 mm, (b) 1 mm and (c) 2 mm. Circles represent straight electrodes, down triangles are 200 μm and up triangles are 250 μm structured electrodes.

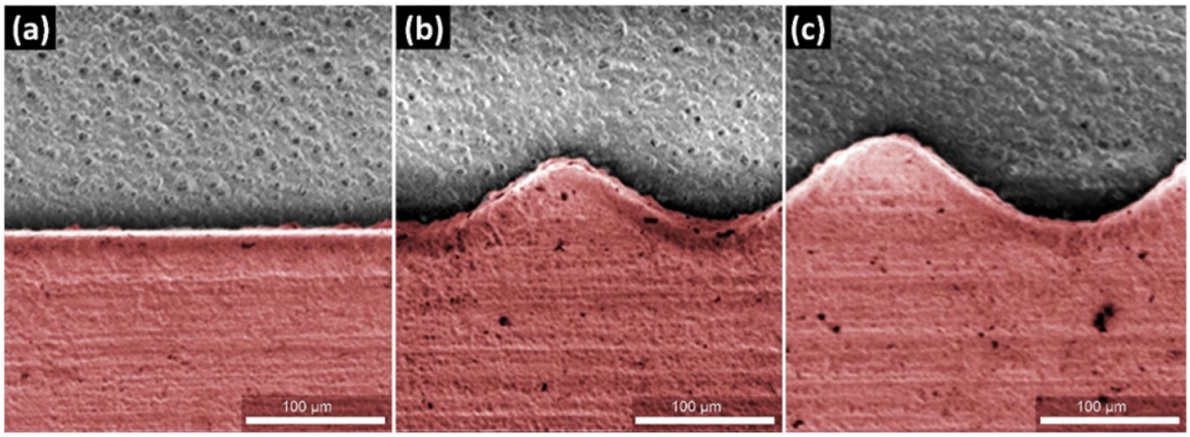

Figure 7. SEM images of three electrodes prior to first operation (red color marks the electrodes): straight design (a), 200 μm design (b), and 250 μm design (c). Compare to figure 8 (electrodes after usage).

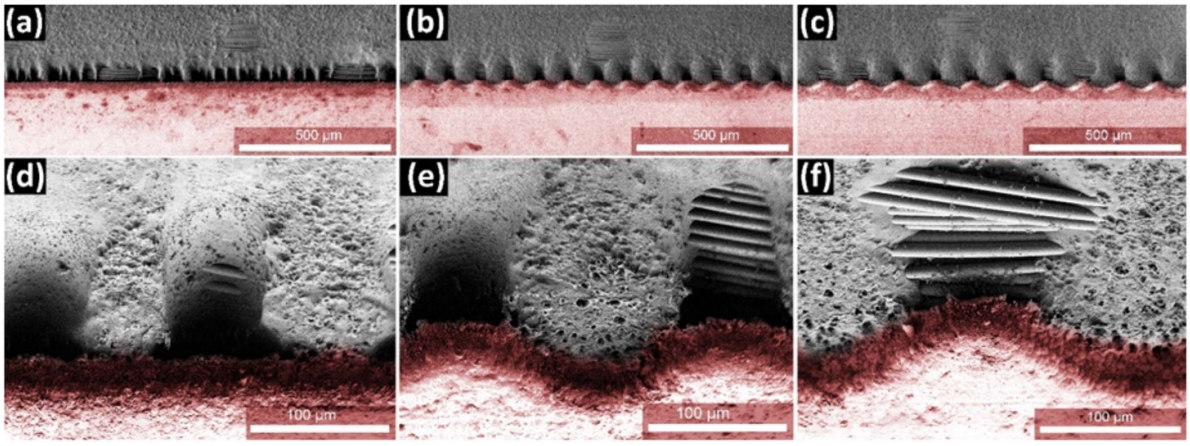

Figure 8. SEM images of three electrode designs (red color marks the electrodes): straight ((a), (d), 200 μm (b), (e), and 250 μm (c), (f). Erosion patterns of dielectrics (upper parts in (a)–(c)) and the local pitting erosion at the electrode edges (zoomed micrographs (d)–(f)) after continuous discharge operation of one hour.

low powers. This agrees with Jolibois and Moreau [24] and with figure 4(b), where a higher value of the dynamic pressure at the same plasma power was obtained. Important to note, that in figure 5(a) the efficiency approaches a saturation above 0.3 W. Since the maximum voltage amplitude was limited in the present experimental setup, the effect could not be validated for higher electrical power consumptions for the thick dielectrics.

For further analysis, the same experimental data are plotted as a function of voltage in figure 5(b). The influence of the ratio p_d/P on the dielectric thickness diminishes here in contrast to figure 5(a). This leads to the conclusion that the amplitude of the applied voltage is crucial for an efficient ion wind generation. SDBDs with thicker dielectrics require higher operation voltages, thus, providing a higher efficiency at low power where the actuator effect is low. It seems that the difference

in the efficiency caused by dielectric thickness is insignificant when the generation of remarkable airflow (> 1 Pa) is achieved.

The data in figures 5 (a) and (b) were measured at one location of the Pitot tube, namely 7 mm apart from the high voltage electrode and near the dielectric surface. The space resolved Pitot tube measurements for the 200 μm structured samples are plotted in figure 5(c) for one selected power and voltage amplitude. At constant power, the efficiency of the actuator with thicker dielectric is higher for all distances from the high voltage electrode, whereas at constant voltage the efficiency of the SDBDs is similar. The deviation for the 2 mm thick SDBD near the high voltage electrode may be explained by a broader velocity profile of the ion wind over the surface. Probably, for thinner dielectrics the maximum velocity is closer to the surface. Then, the stream lines can be disturbed by the Pitot tube wall of 0.5 mm, which can lead to an underestimation of the maximal dynamic pressure for narrow velocity profiles. The velocity profiles becomes broader with increasing the distance to the high voltage, hence the efficiency curves merge.

For a more reliable comparison of the electrode structure, the efficiency as a function of applied voltage is shown for all discharge geometries in figure 6. The straight electrode provides systematically lower efficiency in comparison to electrodes with 250 μm structure. The efficiency for electrodes with 200 μm structure are always in the middle. The electrode structure has a more significant influence if the SDBD is composed by thin dielectrics.

3.5. Surface analysis and material degradation

The material degradation of the SDBDs was investigated using a scanning electron microscope (SEM; instrument: Jeol JSM 7500 F). The SEM employs a field emission gun and a secondary electron in-lens detector enabling the observation of a specimen at a maximum specified resolution of 1.0 nm. Here, the images of the samples were taken with the help of secondary electron imaging (SEI) at 2 kV without conductive coating of the surface. This allows the visualization without artificial effects caused by the sample preparation. A SEI detector taking emitted electrons at a declination angle of 40 degrees has been used. Therefore, the SEM imaging setting is appropriate for 3D samples with a complex perspective in the observation field. In particular, details of electrodes and their interfaces with the dielectric material can be imaged.

Figures 7(a)–(c) present SEM images of samples prior to operation and figures 8(a)–(f) the eroded samples. The samples are degraded by continuous plasma operation of one hour at 5.3 kV_{RMS} with a power consumption of about 0.7 W. The degradation of the dielectric is a result of the plasma generated chemical active species and charged particles which are interacting with the surface. The locations, where the resin material was removed, appear darker in figure 8 and are mainly located near the electrode edge, where the discharge is most intense (see also discharge images in figure 2). At the structured electrodes, erosion channels are aligned to the tips of the electrode structure whereas erosion near the straight electrode does not have a regular structure. At some positions, the woven fiberglass is uncovered as seen by the horizontal parallel lines in figures 8(a)–(f). A minor change is visible at the copper electrodes at the interface to the FR-4 material.

This observation demonstrates the strong degradation of the organic materials under discharge operation. Removing resin near the exposed electrode can lead to an electrical shortcut. Therefore, it was problematic to use 0.2 mm thick PCB actuators for systematic investigations. Poor resistance of organic materials (polyamides, resin) against aggressive plasma environment is well known [22, 26]. However, in the present work the main erosion channels were aligned to the regular pattern of the electrode microstructure. This can be important for fabrication of multifunctional surfaces where an actuator is combined with a riblet structure [21] for aerodynamic drag reduction. Namely, the most intense discharge parts can be placed away from the resin riblet structure to reduce its degradation.

4. Discussion

The data confirm that the electrode microstructure has a influence on the discharge performance. However, a much larger effect was observed by Thomas *et al* [14] for much larger structures (3.2 x 12.7 mm isosceles triangle), where even about 40% decrease of the discharge ignition voltage was obtained. The peak-to-peak ignition voltage for straight electrode of 25 kV (17.7 kV_{RMS}) and for the serrated electrodes of 15 kV (10.6 kV_{RMS}) were roughly estimated from figure 18 in [14]. This drastic difference between the present work and the work of Thomas *et al* [14] is most likely due to the geometric differences of the electrode structures.

The increase of the ion wind with the size of the electrode structure observed in the present work together with the fact that millimetre size structures provide a much stronger effect favours the assumption that the size of the structure plays a crucial role. Whether the structure size is large or small depends on the characteristic size of the discharge, which is the distance between the electrodes or the dielectric thickness. The diminishing of the microstructure effect with the dielectric thickness in figures 4(b) and 6 supports this assumption.

Another effecting parameter is the angle of the triangle structure. The work of [14] claims that on the base of empirical observations the optimum angle is 14°. In the present work, an angle of 90° is used for the isosceles triangles with a comparable thickness of the electrodes (40 μm in [14] and 35 μm in the present work) However, the angle might influence two parameters, namely the radius of curvature of the electrode edge as well as the ratio between structure length and width. The radius of curvature influences directly the electric field amplitude on the electrode tip. It is about 30 μm in present work, estimated from figure 7 and limited by the manufacturing technology anyhow. The value is comparable with the electrode thickness. The radius of curvature parameter was not given in [14]. The ratio of the structure length and width could also influence the electrode electric field configuration. However, too sharp and too thin structures lead to a concentration of the discharge footprints and consequently to a faster erosion of the electrode material.

The third crucial parameter is the gap between the upper exposed high-voltage electrode and the lower embedded ground electrode. In [14] an overlap of the electrodes about the half-dielectric thickness of 3.18 mm was applied while in the present work, the counterpart edges of both electrodes coincide without any distance.

The actuator of [19] had a comparable geometry to one of our experiment: 1 mm of dielectric thickness (glass-fiber-reinforced-epoxy); electrode thickness of 20-40 μm for straight electrodes. The microstructured electrode consisted of 25 μm cutted wires, sticking out about 125 μm from a mesh. The enhancement of the ion wind by the structured electrode was about 50% . Obviously, these thin wires provide much sharper edges in comparison to our experiment in particular, and to the straight electrode of the same thickness. Furthermore, the ratio of its width and length differs significantly.

In the present work about 30% of ion wind enhancement by microstructure implementation can be stated, see figure 3(a), set 1 and set 3, figure 4. However, the scattering and reproducibility of the data points, figures 3(c) and 6, are in the same range. This might be caused by the high spatial resolution of our pressure measurements compared to [14, 19] where the thrust was determined over the full width of the electrode.

Furthermore, the degradation of the electrodes and the dielectric (or status of the surface in general) with operation time, which was not considered in [14, 19], has to be taking into account. In the present work the high voltage amplitude was first increased and then decreased gradually to obtain two data sets per configuration. For all Pitot tube pressure curves a slight deviation was obtained between increasing and decreasing voltage data sets. Obviously, the degradation of the organic dielectrics, see figures 7 and 8, can affect the overall performance after short operation time. Furthermore, our day-to-day and sample-to-sample variation (see e.g. figure 3(c)) gives a deviation of up to 20%. Therefore, we consider the effects of the electrode structure in [14, 19] rather as qualitative then as quantitative.

Comparing the actuator efficiency for the different geometries as a function of applied voltage amplitude, see figure 5, it becomes obvious that larger dielectric thickness has some positive effect on the efficiency. This could be a result of broader velocity profile above the surface [24] and, therefore, the lower wall friction, which consumes up to 30% of the induced momentum close to the wall [25, 29]. The increase of the efficiency for the structured electrodes, figure 6, should be attributed to its size as the curvatures of the 200 μm and 250 μm triangles are the same.

5. Summary

The effects of microstructured exposed electrodes on the power consumption and the ion wind generation of surface DBDs were investigated. The shape of the microstructured electrode and the thickness of the dielectric barrier have been varied systematically. It was shown that the actuator efficiency for ion wind generation grows with the applied voltage. The growth is similar for all investigated samples and a maximum efficiency of about 10 Pa/W was measured at a maximum power consumption per electrode length of about 40 W/m. Thinner dielectrics allow to operate actuators at lower voltages. In particular, it was observed, that a doubling of the dielectric thickness requires an increase of the operation voltage on 15% in order to obtain the same dynamic pressure. A logarithmic dependence of the operation voltage on the dielectric thickness was suggested. The structured electrodes provide an increase of the efficiency for ion wind generation of samples with thin dielectrics of a few percent, but the effect diminishes with larger dielectric thicknesses. A reliable effect of the electrode structure can be achieved if the characteristic length of the structure is comparable with the dielectric thickness. Thus, the investigated 200 and 250 μm structures with 90° angle does not allow to enhance the ion wind significantly in contrast to the 3.2 $\times$ 12.7 mm structure with an angle of 14°. For this situation an increase of the thrust of more than 30% was reported by Thomas *et al* [14].

The electrode structure can distribute the most intense discharge parts by varying the distance between grounded and high voltage electrode. Spots with strong emission are identical with the positions of the erosion channels on the dielectric. Scanning electron microscope images indicate separate erosion sites for 200 and 250 μm electrode structures, but not for straight ones.

Commercially produced printed circuit boards provided reliable micro-scale SDBD samples for systematic studies. The use of multiple actuator samples with the identical design indicates that the reproducibility of the results can be significantly affected by the change of humidity in ambient air and the state of the dielectric surface.

Acknowledgment

Most of the experimental work was performed in the framework of a project funded by Airbus Defence and Space. The authors greatly acknowledge their fellow researchers at INP Greifswald, Markus M Becker and Florian Sigeneger for scientific discussions and Michael Schmidt for technical support.

ORCID iDs

A V Pipa https://orcid.org/0000-0002-1756-1635
J Schäfer https://orcid.org/0000-0002-0652-5057
R Brandenburg https://orcid.org/0000-0003-3153-8439

References

[1] Benard N and Moreau E 2014 Electrical and mechanical characteristics of surface AC dielectric barrier discharge plasma actuators applied to airflow control *Exp. Fluids* **55** 1846
[2] Kriegseis J, Simon B and Grundmann S 2016 Towards in-flight applications? A review on DBD-based boundary-layer control *Appl. Mech. Rev.* **68** 020802
[3] Kotsonis M 2015 Diagnostics for characterisation of plasma actuators *Meas. Sci. Technol.* **26** 092001

[4] Thomas F O, Corke T C, Duong A, Midya S and Yates K 2019 Turbulent drag reduction using pulsed-DC plasma actuation *J. Phys. D: Appl. Phys.* **52** 434001
[5] Rodrigues F, Mushyam A, Pascoa J and Trancossi M 2019 A new plasma actuator configuration for improved efficiency: the stair-shaped dielectric barrier discharge actuator *J. Phys. D: Appl. Phys.* **52** 385201
[6] Samimy M, Webb N and Esfahani A 2019 Reinventing the wheel: excitation of flow instabilities for active flow control using plasma actuators *J. Phys. D: Appl. Phys.* **52** 354002
[7] Sokolova M V, Voevodin V V, Malakhov J I, Aleksandrov N L, Anokhin E M and Soloviev V R 2019 Barrier properties influence on the surface dielectric barrier discharge driven by single voltage pulses of different duration *J. Phys. D: Appl. Phys.* **52** 324001
[8] Post M L and Corke T C 2004 Separation control on high angle of attack airfoil using plasma actuators *AIAA J.* **42** 2177–84
[9] Kriegseis J, Grundmann S and Tropea C 2011 Power consumption, discharge capacitance and light emission as measures for thrust production of dielectric barrier discharge plasma actuators *J. Appl. Phys.* **110** 013305
[10] Schlichting H and Gersten K 2017 *Boundary-Layer Theory* 9th edn (Berlin: Springer)
[11] Xu S Y, Kang L, Cai J S and Tang S J 2018 Experimental investigation on the optical emission spectroscopy of dielectric barrier discharge plasma actuators at different atmospheric pressures *AIP Adv.* **8** 115033
[12] Duchmann A, Simon B, Tropea C and Grundmann S 2014 Dielectric barrier discharge plasma actuators for in-flight transition delay *AIAA J.* **52** 358–67
[13] Zhu Y, Wu Y, Wei B, Xu H, Liang H, Jia M, Song H and Li Y 2020 Nanosecond-pulsed dielectric barrier discharge-based plasma-assisted anti-icing: modeling and mechanism analysis *J. Phys. D: Appl. Phys.* **53** 145205
[14] Thomas F, Corke T, Iqbal M, Kozlov A and Schatzman D 2009 Optimization of dielectric discharge plasma actuators for active aerodynamic flow control *AIAA J.* **47** 2169–78
[15] Forte M, Jolibois J, Pons J, Moreau E, Touchard G and Cazalens M 2007 Optimization of a dielectric barrier discharge actuator by stationary and non-stationary measurements of the induced flow velocity: application to airflow control *Exp. Fluids* **43** 917–28
[16] Neretti G, Seri P, Taglioli M, Shaw A, Iza F and Borghi C A 2017 Geometry optimization of linear and annular plasma synthetic jet actuators *J. Phys. D: Appl. Phys.* **50** 015210
[17] Sato S, Furukawa H, Komuro A, Takahashi M and Ohnishi N 2019 Successively accelerated ionic wind with integrated dielectric-barrier-discharge plasma actuator for low-voltage operation *Sci. Rep.* **9** 5813
[18] Debien A, Benard N and Moreau E 2012 Streamer inhibition for improving force and electric wind produced by DBD actuators *J. Phys. D: Appl. Phys.* **45** 215201
[19] Abe T, Takizawa Y and Sato S 2008 Experimental study for momentum transfer in a dielectric barrier discharge plasma actuator *AIAA J.* **46** 2249–56
[20] Lindner M *et al* 2019 Fabrication, surface integration and testing of miniaturized dielectric barrier discharge plasma actuators for active flow control applications *AIAA Aviation Forum* p 2998
[21] Berndt D *et al* 2019 Max A and Caspari R Realization of multifunctional surfaces containing MEMS-based DBD plasma actuators and biomimetic structures for flow manipulation *AIAA Aviation Forum* p 2999
[22] Bian D, Wu Y, Long C and Lin B 2018 Effects of material degradation on electrical and optical characteristics of surface dielectric barrier discharge *J. Appl. Phys.* **124** 183301
[23] Pipa A V and Brandenburg R 2019 The equivalent circuit approach for the electrical diagnostics of dielectric barrier discharges: the classical theory and recent developments *Atoms* **7** 14
[24] Jolibois E and Moreau E 2009 Enhancement of the electromechanical performances of a single dielectric barrier discharge actuator *IEEE Trans. Dielectr. Electr. Insul.* **16** 0758
[25] Kriegseis J, Schwarz C, Duchmann A, Grundmann S and Tropea C 2012 PIV-based estimation of DBD plasma-actuator force terms *AIAA Aerospace Sciences Meeting including the New Horizons Forum and Aerospace Exposition (Nashville, Tennessee)* vol 50 p 411
[26] Houser N, Gimeno L, Hanson R, Goldhawk T, Simpson T and Lavoie P 2013 Microfabrication of dielectric barrier discharge plasma actuators for flow control *Sensors Actuators* A **201** 101–4
[27] Berendt A, Podliński J and Mizeraczyk J 2011 Comparison of airflow patterns produced by DBD actuators with smooth or saw-like discharge electrode *J. Phys.: Conf. Ser.* **301** 012018
[28] Joussot R, Leroy A, Weber R, Rabat H, Loyer S and Hong D 2013 Plasma morphology and induced airflow characterization of a DBD actuator with serrated electrode *J. Phys. D: Appl. Phys.* **46** 125204
[29] Enloe C L, McHarg M G, Font G I and McLaughlin T E 2009 Plasma-induced force and self-induced drag in the dielectric barrier discharge aerodynamic plasma actuator *47th AIAA Aerospace Sciences Meeting Including The New Horizons Forum and Aerospace Exposition (Orlando, Florida)* p 1622